Acta Cryst E CRYSTALLOGRAPHIC COMMUNICATIONS

ISSN 2056-9890

A strongly fluorescent Ni^{II} complex with 2-(2-hydroxyethyl)pyridine ligands: synthesis, characterization and theoretical analysis and comparison with a related polymeric Cu^{II} complex

Ouahida Zeghouan,[a,b]* Mohamed AbdEsselem Dems,[c,b] Seifeddine Sellami,[d] Hocine Merazig[a] and Jean Claude Daran[e]

[a]Unité de Recherche Chimie de l'Environnement et Moléculaire Structurale, 'CHEMS', Faculté des Sciences Exactes, Campus Chaabet Ersas, Université Frères Mentouri Constantine 1, 25000 Constantine, Algeria, [b]Centre de Recherche en Biotechnologie, Constantine, Algeria, [c]Laboratoire de Chimie des Matériaux et des Vivants: Activité, Réactivité, Université Hadj-Lakhdar Batna, Algeria, [d]Laboratoire Pollution et Traitement des Eaux, Département de Chimie, Faculté des Sciences Exactes, Université Frères Mentouri Constantine 1, 25000 Constantine, Algeria, and [e]Laboratoire de Chimie de Coordination, UPR-CNRS 8241, 205 route de Narbonne, 31077 Toulouse Cedex 4, France. *Correspondence e-mail: ouahida.zeghouan@gmail.com

Received 5 June 2018
Accepted 27 June 2018

Edited by A. Van der Lee, Université de Montpellier II, France

Keywords: transition metal; fluorescence; blue-light emission; TDDFT; crystal structure.

CCDC reference: 1481640

Supporting information: this article has supporting information at journals.iucr.org/e

The synthesis and characterization of diaquabis[2-(2-hydroxyethyl)pyridine-κ^2N,O)nickel(II) dinitrate, $[Ni(C_7H_9NO)_2(H_2O)_2](NO_3)_2$, under ambient conditions is reported and compared with *catena*-poly[[bis[2-(2-hydroxyethyl)-pyridine-κ^2N,O]copper(II)]-μ-sulfato-$\kappa^2O:O'$], $[Cu(C_7H_9NO)_2(SO_4)]_n$ [Zeghouan *et al.* (2016). Private communication (refcode 1481676). CCDC, Cambridge, England]. In the two complexes, the 2-(2-hydroxyethyl)pyridine ligands coordinate the metal ions through the N atom of the pyridine ring and the O atom of the hydroxy group, creating a chelate ring. The Ni^{II} or Cu^{II} ion lies on an inversion centre and exhibits a slightly distorted MO_4N_2 octahedral coordination geometry, build up by O and N atoms from two 2-(2-hydroxyethyl)pyridine ligands and two water molecules or two O atoms belonging to sulfate anions. The sulfate anion bridges the Cu^{II} ions, forming a polymeric chain. The photoluminescence properties of these complexes have been studied on as-synthesized samples and reveal that both compounds display a strong blue-light emission with maxima around 497 nm. From DFT/TDDFT studies, the blue emission appears to be derived from the ligand-to-metal charge-transfer (LMCT) excited state. In addition, the IR spectroscopic properties and thermogravimetric behaviours of both complexes have been investigated.

1. Chemical context

A wide variety of nitrogen-containing heterocyclic ligands has been used to construct coordination complexes (Lin *et al.*, 2015; Kim *et al.*, 2015; Huang *et al.*, 2015). In particular, pyridine alcohol derivatives and their metal complexes have been studied extensively in recent years, focusing on the rational design and synthesis of coordination monomers and polymers because of their intriguing structural features as well as potential applications in catalysis and fluorescence and as chemical sensors (Ley *et al.*, 2010). Moreover, luminescent compounds have also attracted attention because of their applications, particularly in modern electronics, as materials for producing organic light-emitting diodes (OLEDs) (Kelley *et al.*, 2004). The 2-(2-hydroxyethyl)pyridine (hep-H) ligand may adopt many coordinating variants because of its donating capabilities: *N*-monodentate (*N*) (Martínez *et al.*, 2007), *N*,*O*-chelating ($^2N,O$) (Antonioli *et al.*, 2007); deprotonated

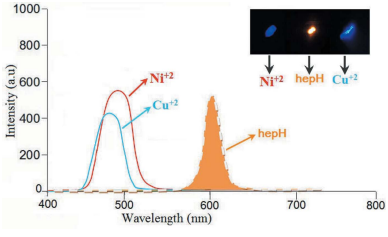

chelating ($^2N,O$) (Antonioli *et al.*, 2007) and bridging (N:O) (Antonioli *et al.*, 2007), $^2N,O$:$O^7$and $^2N,O$:O:O (Wang *et al.*, 2010) or simultaneously $^2N,O$:O and $^2N,O$:O:O bridging (Stamatatos, Boudalis *et al.*, 2007).

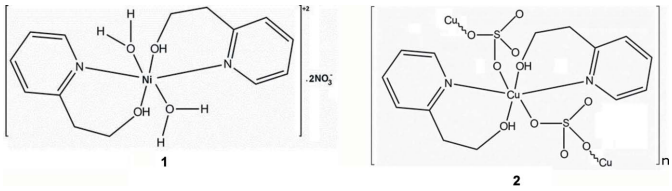

1 2

We are in particular interested in the hep-H ligand, which has attracted much attention in biology and chemistry because it is a useful model and for its practical applications (Kong *et al.*, 2009; Mobin *et al.*, 2010). The hep-H ligand could be a good candidate to construct simultaneously nitrogen heteroaromatic alcohol coordination monomers and polymers with interesting magnetic behaviour. On the other hand, with Ni^{II} and Cu^{II} metals, the hep-H ligand could also be a desirable candidate for fluorescent materials. The flexible coordination sphere around the Ni^{II} and Cu^{II} ions, in combination with steric and packing forces, is one of the effects that gives rise to a wide structural diversity in Ni^{II}/Cu^{II} coordination chemistry (Comba & Remenyi, 2003).

The combination of multidentate ligands with suitable cations has led to a large number of novel mononuclear and polynuclear complexes. In this study, by reacting the flexible hep-H ligand with $Ni(NO_3)_2{\cdot}6H_2O$, we have successfully obtained the monomeric Ni^{II} complex diaquabis[2-(2-hydroxyethyl)pyridine-κ^2N,O)nickel(II) dinitrate, $[Ni(C_7H_8NO)_2(H_2O)_2](NO_3)_2$ (**1**). The related polymeric complex, *catena*-poly[[bis[2-(2-hydroxyethyl)pyridine-κ^2N,O]copper(II)]-μ-sulfato-κ^2O:O'], $[Cu(C_7H_8NO)_2(SO_4)]_n$ (Zeghouan *et al.*, 2016; Zienkiewicz-Machnik *et al.*, 2016) had previously been obtained by reacting the hep-H ligand with $Cu(SO_4)_2{\cdot}6H_2O$. Herein we compare their structures, IR spectra, thermostability, fluorescence and absorption properties and tge results of a theoretical study performed using TDDFT calculations.

2. Structural commentary

In the mononuclear title Ni^{II} complex **1** as well as in the polymeric Cu^{II} complex **2** (Zeghouan *et al.*, 2016; Zienkiewicz-Machnik *et al.*, 2016), the metal ions are located on inversion centers with the neutral hep-H molecule acting as a bidentate ligand in a $^2N,O$ fashion and forming the equatorial plane of an octahedron, the apex of which is occupied by the water molecules in the case of the Ni^{II} complex or an O atom of an SO_4^{2-} anion in the Cu^{II} complex (Figs. 1 and 2). The main difference between the two structures is the occurrence of the SO_4^{2-} anion in **2**, which links complex molecules, forming a polymeric chain. Moreover, in this structure the asymmetric unit contains two half molecules of the complex. In the Ni^{II} complex, two nitrate anions balance the charges. The coordination environment around the nickel ions can be described as a nearly perfect octahedron. The O1—Ni1—N1 [88.68 (3)°], N1—Ni1—O1*W* [90.00 (4)°] and O1—Ni1—O1*W* [89.26 (4)°] angles are all very close to 90° (Table 1). The two hep-H ligands are *trans* with respect to each other. The hydroxyl O atom and the pyridine N atoms define the equatorial plane while the water molecules occupy the apices. In the case of the Cu^{II} complex, the octahedron is slightly distorted with the angles around the metal ranging from 83.39 (5) to 96.62 (5)°. This distortion might result from the influence of the SO_4^{2-} linking the Cu complex to form a polymeric chain.

In both complexes, the chelate ring displays a twist-boat conformation with puckering parameters θ = 81.9° and φ = 162° for **1** and θ = 79.2° and φ = 159.9° and θ = 87.75° and φ= 176.08° for the two molecules of **2**.

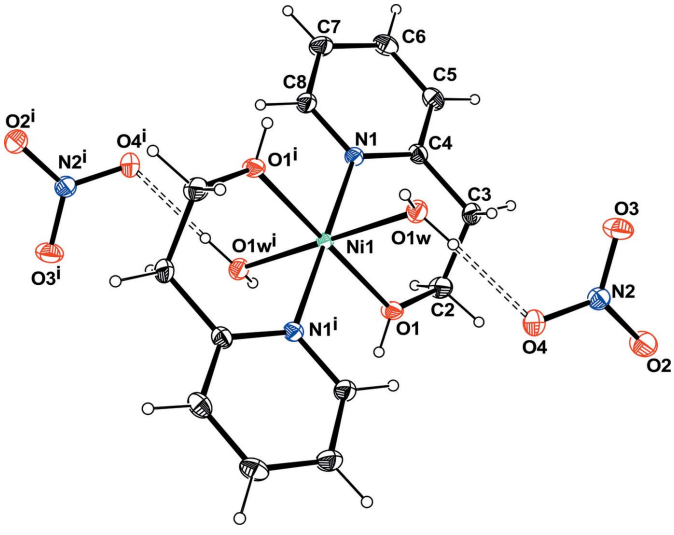

Figure 1
View of the Ni complex, with the atom-numbering scheme. Displacement ellipsoids are drawn at the 50% probability level and H atoms are shown as circles of arbitrary radii. Hydrogen bonds are shown as dashed lines. [Symmetry code: (i): $-x+1, -y+1, -z+2$].

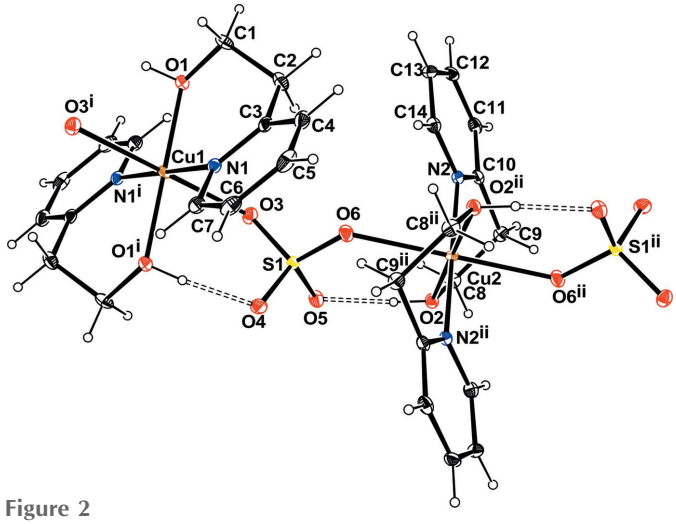

Figure 2
Partial view of the polymer chain in the Cu compound, with displacement ellipsoids drawn at the 50% probability level. Hydrogen bonds are shown as dashed lines. [Symmetry code: (i) $-x+1, -y+2, -z+2$; (ii) $-x, -y+1, -z+1$].

Table 1
Comparison of experimental and calculated distances and angles (Å, °) in **1** and **2**.

1		
Ni1—O1	2.0622 (14)	2.07
Ni1—O1*W*	2.0831 (15)	2.10
Ni1—N1	2.1019 (14)	2.12
O2—N2	1.2520 (14)	1.23
O3—N2	1.2548 (12)	1.22
O4—N2	1.2537 (12)	1.27
O1—Ni1—O1*W*	90.74 (4)	93.00
O1—Ni1—N1	88.68 (3)	87.00
O1—Ni1—O1*W*^{i}	89.26 (4)	91.8
O1—Ni1—N1^{i}	91.32 (3)	92.3
O1*W*—Ni1—N1	90.00 (4)	92
O1^{i}—Ni1—O1*W*	89.26 (4)	87.00
O1*W*—Ni1—N1^{i}	90.00 (4)	91.8
O1^{i}—Ni1—N1	91.32 (3)	92.3
O1*W*^{i}—Ni1—N1	90.00 (4)	91.8
O1^{i}—Ni1—O1*W*^{i}	90.74 (4)	87.5
O1*W*—Ni1—O1—C2	−79.99 (10)	80.02
N1^{i}—Ni1—O1—C2	−170.01 (10)	166.70
O1—Ni1—N1—C4	−29.33 (10)	31.30
O1—Ni1—N1—C8	151.96 (9)	−147.60
O1*W*^{i}—Ni1—N1—C4	−118.59 (9)	114.9
O1*W*^{i}—Ni1—N1—C8	62.70 (9)	−64.00
2		
Cu1—O1	2.01	2.08
Cu1—N1	2.02	1.99
Cu1—O1^{i}	2.01	2.08
Cu1—N1^{i}	2.02	1.99
Cu2—O2	2.05	2.08
N2—Cu2—N2^{ii}	180	180.00
O1—Cu1—N1	92.39	90.60
O1—Cu1—O1^{i}	180	180.00
O3—Cu1—O1—C1	−93.9	−98
O1—Cu1—N1—C7	−151.03	−153
N2—Cu2—O2—C8	151.24	148
Cu1—O1—C1—C2	−37.55.	−40
C7—N1—C3—C2	177	179
C7—N1—C3—C4	−0.5	−0.4

3. Supramolecular features

Although not coordinated to the Ni atom, the nitrate anion in **1** participates in the packing motif. The hydroxyl group and water molecules are involved in strong O—H···O hydrogen bonds (Table 2) with the O atoms of the nitrate anions, resulting in the formation of $R_4^4(12)$ and $R_4^4(16)$ graph-set motifs, as shown in Fig. 3, building up a three-dimensional network. C—H···O hydrogen bonds also occur.

4. Database survey

A search of the Cambridge Structural Database (CSD, Version 5.36; Groom *et al.*, 2016) based on an Ni(hep-H)$_2$O$_2$ fragment gave 11 hits for closely related structures with an octahedral Ni complex, located on an inversion center, coordinated by two chelating *N*,*O* hep-H ligands in the equatorial plane and two O atoms of different ligands at the apices. A comparison of the Ni—N and Ni—O bond lengths as well as of the dihedral angles between the equatorial NiO$_2$N$_2$ plane and the pyridine ring is displayed in Table 3. There are no notable differences between the Ni—O(H) distances, which range from 2.057 (2) to 2.114 (1) Å, and the Ni—O(ligand) bonds, ranging from 2.052 (1) to 2.112 (2) Å. Clearly the organic substituent attached to the O atom in the axial position has no real influence on the Ni—O(*R*) bond length. The dihedral angles between the pyridine ring and the NiN$_2$O$_2$ basal square plane range from 28.3 to 37.6°. The largest angle is observed for two polymeric structures in which the succinato or adipato organic ligand bridge the Ni atoms, forming a chain; this is possibly related to steric effects. A similar search on the Cu(Hep-H)$_2$O$_2$ fragment gave seven hits. The major differ-

Table 2
Hydrogen-bond geometry (Å, °).

D—H···*A*	*D*—H	H···*A*	*D*···*A*	*D*—H···*A*
O1*W*—H2*W*···O3^{i}	0.84	1.95	2.7870 (16)	176
O1*W*—H2*W*···N2^{i}	0.84	2.68	3.455 (2)	153
O1*W*—H1*W*···O4	0.85	1.93	2.7720 (19)	174
O1—H1···O2^{ii}	0.82	1.88	2.6952 (15)	172
O1—H1···N2^{ii}	0.82	2.65	3.4208 (17)	159
C2—H2*B*···O3^{iii}	0.97	2.64	3.378 (2)	133
C3—H3*A*···O1*W*	0.97	2.55	3.2278 (17)	127
C8—H8···O1^{iv}	0.93	2.49	3.0136 (19)	116
C8—H8···O4^{iv}	0.93	2.66	3.4448 (18)	143
C5—H5···O2^{v}	0.93	2.41	3.3076 (19)	163

Symmetry codes: (i) $-x+2, -y+1, -z+2$; (ii) $-x+1, -y, -z+2$; (iii) $x-1, y, z$; (iv) $-x+1, -y+1, -z+2$; (v) $-x+1, -y, -z+1$.

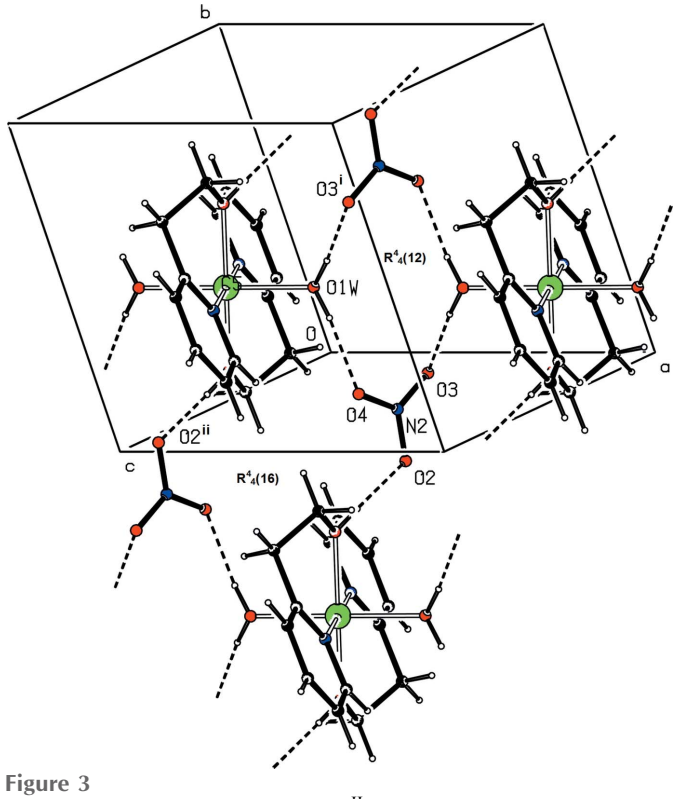

Figure 3
Partial view of the packing in the Ni^{II} complex showing the O—H···O hydrogen bonds (dashed lines) and the formation of the $R_4^4(12)$ and $R_4^4(16)$ graph-set motifs. [Symmetry codes: (i) $-x+2, -y+1, -z+2$; (ii) $-x+1, -y, -z+2$].

Table 3
Comparison of selected geometrical parameters (%, Å, °) for Ni^{II} and Cu^{II} complexes bearing the hep-H ligand.

Δ is the dihedral angle between the basal MO_2N_2 square plane and the pyridine ring.

Ref.	*R*-factor	*M*—N	*M*—OH	*M*—O(*R*)	Δ	θ	φ
1	1.80	2.102 (1)	2.062 (1)	2.083 (2)	28.28 (4)	81.9 (1)	162.6 (1)
BOZJAD[a]	3.80	2.102 (2)	2.065 (3)	2.084 (3)	28.4 (1)	80.6 (3)	163.4 (3)
HULYAO[b]	3.22	2.073 (1)	2.064 (1)	2.085 (1)	30.37 (6)	78.7 (1)	156.3 (1)
EJEZEZ[c]	2.58	2.082 (1)	2.089 (1)	2.090 (1)	30.88 (6)	99.0 (1)	346.8 (1)
FEFWIY[d]	3.13	2.100 (2)	2.088 (1)	2.072 (2)	30.4 (1)	96.8 (2)	349.7 (2)
FEFWIY01[d]	3.05	2.090 (1)	2.104 (1)	2.064 (1)	31.86 (8)	95.9 (1)	354.6 (2)
FEFWIY02[d]	2.59	2.096 (1)	2.085 (1)	2.064 (1)	30.51 (7)	97.9 (1)	346.1 (1)
BOZJOR[a]	3.75	2.078 (2)	2.096 (1)	2.063 (2)	37.6 (1)	89.2 (2)	175.3 (2)
BOZJUX[a]	3.03	2.083 (1)	2.114 (1)	2.052 (1)	35.43 (8)	94.3 (1)	352.5 (2)
BOZKAE[a]	4.36	2.098 (2)	2.096 (2)	2.064 (2)	29.9 (1)	81.9 (2)	160.4 (2)
RAJQOL[e]	4.07	2.083 (2)	2.057 (2)	2.112 (2)	31.9 (1)	84.5 (2)	167.7 (2)
2 NABBEA01[f]	1.9	2.025 (2) 1.988 (2)	2.012 (2) 2.055 (1)	2.380 (1) 2.298 (1)	28.5 (1) 38.0 (1)	79.2 (1) 87.8 (1)	159.9 (1) 176.2 (1)
NABBEA[g]	5.2	1.993 (4) 2.031 (4)	2.070 (4) 2.016 (4)	2.298 (4) 2.387 (4)	37.5 (2) 28.8 (2)	87.5 (3) 100.3 (4)	175.9 (3) 340.6 (4)
HAYHAS[h]	2.8	2.032 (2)	2.422 (1)	1.982 (1)	29.50 (7)	81.9 (1)	171.9 (1)
IRERED[i]	4.04	2.017 (2)	2.385 (2)	2.025 (2)	31.0 (1)	94.4 (2)	356.0 (2)
OJOBAQ[j]	2.35	2.009 (1)	2.041 (1)	2.312 (1)	33.96 (4)	98.6 (1)	340.0 (1)
SOJGAB[k]	3.52	2.029 (2)	2.428 (2)	1.998 (1)	25.97 (8)	101.4 (2)	346.6 (2)
UGAROK[l]	3.44	2.021 (2) 2.030 (2)	2.019 (2) 2.024 (2)	2.357 (2) 2.346 (2)	31.4 (1) 32.5 (1)	95.9 (2) 80.6 (2)	345.3 (2) 167.0 (2)

Notes: (*a*) Trdin *et al.* (2015); (*b*) Hamamci *et al.* (2002); (*c*) Yilmaz *et al.* (2011); (*d*) Trdin & Lah (2012); (*e*) Çolak *et al.* (2017); (*f*) Zeghouan *et al.* (2016); (*g*) Zienkiewicz-Machnik *et al.* (2016); (*h*) Lapanje *et al.* (2012); (*i*) Pothiraja *et al.* (2011); (*j*) Yilmaz *et al.* (2003); (*k*) Caglar *et al.* (2014); (*l*) Yeşilel *et al.* (2009).

ence observed with the related Ni complexes is the large discrepancy in the Cu—O(H) bond lengths, which range from 2.012 (2) to 2.428 (2) Å and the Cu—O(*R*) lengths, ranging from 1.982 (1) to 2.387 (4) Å. The difference observed between the Cu—O(H) and Cu—O(*R*) bond lengths might be due to the Jahn–Teller effect. The dihedral angles between the pyridine ring and the CuN_2O_2 basal square plane, ranging from 26 to 38°, are close to those found in the Ni complexes. Similar twist-boat conformations are observed in all of the related Ni and Cu complexes bearing the hep-H ligand (Table 3).

5. Thermogravimetric and differential thermal analysis

Thermal analyses were performed on a SETARM 92-16.18 PC/PG 1 instrument from 303 to 1273 K under a dynamic air atmosphere and under nitrogen at 200.0 ml min^{-1} with a heating rate of 283 K min^{-1}. The stability of the two complexes was measured by TGA and the experimental results are in agreement with the calculated data.

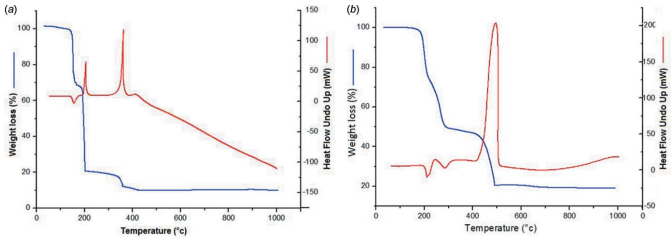

Figure 4
The thermogravimetric (TG) and differential thermal analysis (DTA) curves for (*a*) the monomer and (*b*) the polymer.

The TG curve for **1** (Fig. 4*a*) shows that the monomer is stable up to 424 K with the first weight loss of 33.55% (calculated 34.21%) at 303 −438 K corresponding to the loss of two coordinated water molecules and the organic hep-H ligand. The second loss of 47.51% (calculated 40.02%) at 438–488 K corresponds to the loss of the second hep-H ligand and the nitrate anion, and then the second nitrate anion decomposes (DP/P = 12.14%, calculated =13.34%). In addition, the corresponding endothermic and exothermic peaks (at 424.26, 475.06 and 631.85 K) in the differential scanning ATD curve also record the processes of weight loss. As illustrated in Fig. 4*b*, the TG curve for **2** shows that the polymer is stable up to 470 K with the first weight loss of 24.16% (calculated 23.66%) at 470–483 K corresponding to the loss of the sulfate anion and the second loss of 29.42% (calculated 30.30%) at 483–573 K to the loss of the first hep-H ligand, and then the second hep-H ligand decomposes (DP/P = 28.55%, calculated =30.30%). In addition, the corresponding endothermic and exothermic peaks (at 473, 558 and 773 K) in the differential scanning ATD curve also record the processes of weight loss.

6. Luminescence properties

Photoluminescence spectra were measured using a Cary Eclipse (Agilent Technologies) fluorescence spectrophotometer with quartz cell (1 × 1 cm^2 cross-section) equipped with a xenon lamp and a dual monochromator. The measurements were carried out at ambient temperature (298 K) with the $slit_{ex/em}$ = 10 nm/10 nm. The photoluminescence properties of **1**, **2** and free hep-H in an ethanol–water (*v*/*v* = 1:1) solution were investigated in the visible region. As shown in Fig. 5, free hep-H displays orange emission with a band at 496.06 nm (excited at 269.70 nm), which may be assigned to a π–π^* electronic transition. When hep-H

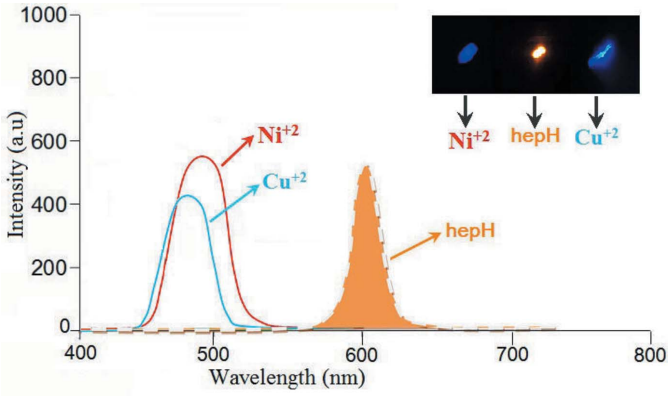

Figure 5
The fluorescence spectrum of the hep-H ligand and the title compounds (excitation at 250 and 269.70 nm for the complexes and hep-H, respectively)

is combined with Ni^{II} or Cu^{II} in **1** or **2**, an intense blue emission band is seen at $\lambda_{em}/\lambda_{ex}$ = 498.03 nm/250.93 nm or 496.96 nm/250.00 nm respectively. This should probably be assigned to the π–π* charge-transfer interaction of the hep-H ligands. The observed blue shift of the emission maximum between **1**, **2** and free hep-H is considered to originate mainly from the influence of the coordination of the metal atoms to the hep-H ligand (Leitl *et al.*, 2016). Thus, these compounds may be candidates for blue-light luminescent materials which suggests that more transition metal, pyridine alcohol compounds with good luminescent properties can be developed.

7. TDDFT calculations

In an effort to better understand the nature of the electronic transitions exhibited by compounds **1** and **2**, DFT calculations using the Amsterdam density function (ADF) software (Baerends *et al.*, 1973) along with generalized gradient approximations, exchange and correlation functional GGA (PBE) (Perdew *et al.*, 1997), employing the TZP (triple zeta polarized) basis set. The singlet excited state was optimized using time-dependent density functional theory calculations (TDDFT) (Bauernschmitt & Ahlrichs, 1996; Gross & Kohn, 1990; Gross *et al.*, 1996).

Table 4
The calculated optical transition energies (nm) and their corresponding oscillator strengths (*f*) (ev) for **1** and **2**.

λ	*f*	*E*	Transition	Type
1				
286	0.03	4.33	HOMO-2 to LUMO	LMTC
280	0.01	4.42	HOMO-3 to LUMO	LMTC
2				
507	0.009	2.44	HOMO-4 to LUMO	LMTC
443	0.08	4.03	HOMO-5 to LUMO	LMTC
244	0.07	5.81	HOMO-2 to LUMO+1	LLTC

The ground-state geometry of **1** and **2** was adapted from the X-ray data. The calculated structural parameters show a good agreement with the original X-ray diffraction data (Table 1); the root-mean-square deviation *f* between the X-ray and the DFT structure for non-hydrogen atoms is 0.603 and 0.620 Å for **1** and **2**, respectively. The computed absorption bands, dominant transitions, characters, and oscillator strengths (*f*) are given in Table 4. As shown in this table, two absorption features are predicted for the monomer; these mainly consist of absorption peaks located at λ = 286 and 280 nm, resulting from the HOMO-2 to LUMO transition and the HOMO-3 to LUMO transition, which is attributed to a ligand–metal charge transfer (LMTC) (Fig. 6*a*). Three absorption features are predicted in the polymer, consisting mainly of absorption peaks that are located at λ = 507, 443 and 244 nm, resulting from HOMO-4 to LUMO, HOMO-5 to LUMO and HOMO-2 to LUMO transitions, which are attributed to a ligand–metal charge transfer (LMTC) (Fig. 6*b*). The HOMO–LUMO energy gap was found to be 4.33, 4.42 for the transitions in **1** and 2.44, 4.03, 5.81 ev for the transitions in **2**.

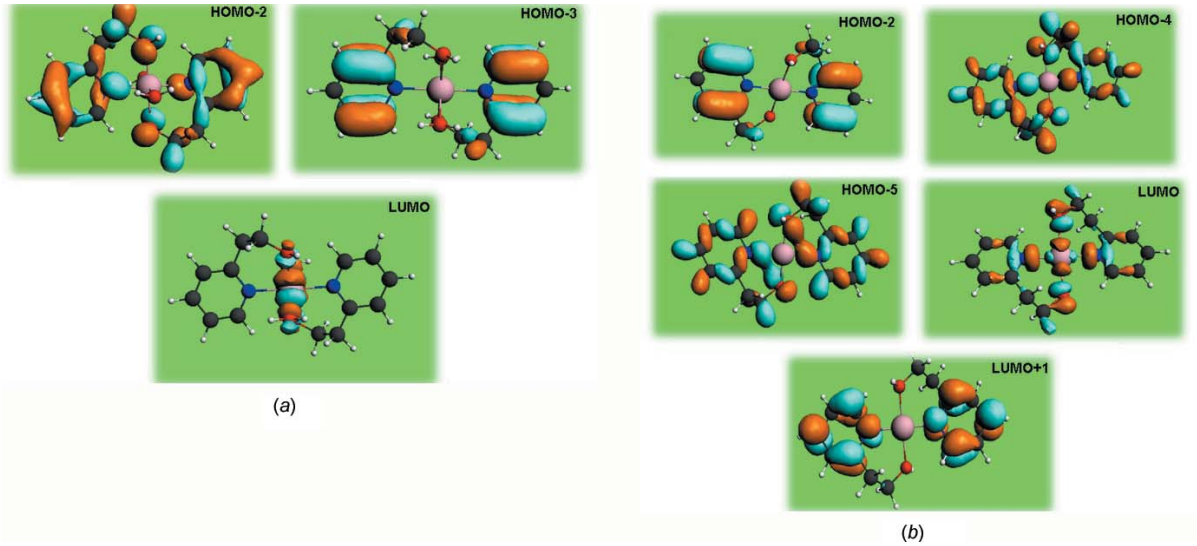

Figure 6
Plots of the molecular orbitals dominating the contribution of the low-energy transitions for (*a*) the monomer and (*b*) the polymer.

8. Synthesis and crystallization

All chemicals and solvents were commercially purchased and used as received. The infrared spectra were recorded on a Perkin–Elmer spectrometer at room temperature in the range of 4000–500 cm^{-1}.

The hep-H ligand was obtained from commercial sources. The synthesis of the two compounds followed the same procedures as previously described for the Co^{II} analog (Zeghouan *et al.*, 2013). (2-Hydroxyethyl)pyridine (10.0 mmol, 1.67 g) was reacted in a mixture of ethanol–water (*v*/*v* = 1:1) with $Ni(NO_3)_2{\cdot}6H_2O$ (10.0 mmol, 2.50 g) for the Ni^{II} analogue and with $Cu(SO_4)_2{\cdot}6H_2O$ (10.0 mmol, 2.3 g) for the Cu^{II} analogue. The solutions were maintained under agitation for 24 h at room temperature. Green prisms of the monomer and green prisms of the polymer were obtained by slow evaporation of the solvents within three weeks. The crystals formed were filtered and washed with 15 ml of water.

IR (cm^{-1}, pure crystals of compounds without KBr): Ni analogue: 3389 (*vs*), 3124 (*vs*), 2862 (*m*), 2764 (*m*), 2360 (*m*), 1658 (*m*), 1442 (*m*), 1371 (*vs*), 1306 (*vs*), 1084 (*m*), 1021 (*m*), 763 (*m*), 586 (*m*). Cu analogue: 3392 (*vs*), 3127 (*s*), 2911 (*m*), 1655 (*m*), 1609 (*m*), 1572 (*w*), 1493 (*w*), 1444 (*w*), 1373 (*vs*), 1356 (*vs*), 1313 (*m*), 1159 (*m*), 1082 (*m*), 1023 (*m*), 907 (*w*), 860 (*s*), 764 (*m*), 706 (*s*), 643 (*s*).

9. Refinement

Crystal data, data collection and structure refinement details are summarized in Table 5. O-bound H atoms were located in a difference-Fourier map and refined with O—H restrained to 0.85 (1) Å, with $U_{iso}(H) = 1.5U_{eq}(O)$. For the water molecule a further H···H distance restraint of 1.39 (2) Å was used. C-bound H atoms were placed at calculated positions with C—H = 0.93 Å (aromatic H atoms) and 0.97 Å (methylene H atoms), and refined in riding mode with $U_{iso}(H) = 1.2U_{eq}(C)$. Four reflections were omitted from the refinement.

Table 5
Experimental details.

Crystal data	
Chemical formula	$[Ni(C_7H_9NO)_2(H_2O)_2](NO_3)_2$
M_r	465.05
Crystal system, space group	Triclinic, $P\overline{1}$
Temperature (K)	293
a, *b*, *c* (Å)	7.782 (5), 8.185 (5), 8.811 (5)
α, β, γ (°)	96.785 (5), 113.856 (5), 109.140 (5)
V (Å^3)	464.0 (5)
Z	1
Radiation type	Mo *Kα*
μ (mm^{-1})	1.11
Crystal size (mm)	0.18 × 0.11 × 0.08
Data collection	
Diffractometer	Bruker APEXII
No. of measured, independent and observed [$I > 2\sigma(I)$] reflections	2478, 2478, 2471
R_{int}	0.019
$(\sin\theta/\lambda)_{max}$ (Å^{-1})	0.685
Refinement	
$R[F^2 > 2\sigma(F^2)]$, $wR(F^2)$, *S*	0.018, 0.051, 1.08
No. of reflections	2478
No. of parameters	133
No. of restraints	4
H-atom treatment	H atoms treated by a mixture of independent and constrained refinement
$\Delta\rho_{max}$, $\Delta\rho_{min}$ (e Å^{-3})	0.42, −0.29

Computer programs: *APEX2* and *SAINT* (Bruker, 2006), *SIR2002* (Burla *et al.*, 2003), *SHELXL* (Sheldrick, 2015), *ORTEPIII* (Burnett & Johnson, 1996), *ORTEP-3 for Windows* and *WinGX* (Farrugia, 2012), *PLATON* (Spek, 2009) and *Mercury* (Macrae *et al.*, 2006).

Funding information

This work was supported by the Unité de Recherche de Chimie de l'Environnement et Moléculaire Structurale (URCHEMS), Université Frères Mentouri Constantine, Algeria and the Biotechnology Research Center (CRBt), Constantine, Algeria. Thanks are due to MESRS and ATRST (Ministère de l'Enseignement Supérieur et de la Recherche Scientifique et l'Agence Thématique de Recherche en Sciences et Technologie, Algeria) for financial support *via* the PNR program.

References

Antonioli, B., Bray, D. J., Clegg, J. K., Jolliffe, K. A., Gloe, K., Gloe, K. & Lindoy, L. F. (2007). *Polyhedron*, **26**, 673–678.

Baerends, E. J., Ellis, D. E. & Ros, P. (1973). *J. Chem. Phys.* **2**(1), 41–51.

Bauernschmitt, R. & Ahlrichs, R. (1996). *J. Chem. Phys.* **104**, 9047–9052.

Bruker (2006). *APEX2* and *SAINT*. Bruker AXS Inc., Madison, Wisconsin, USA.

Burla, M. C., Camalli, M., Carrozzini, B., Cascarano, G. L., Giacovazzo, C., Polidori, G. & Spagna, R. (2003). *J. Appl. Cryst.* **36**, 1103.

Burnett, M. N. & Johnson, C. K. (1996). *ORTEPIII*. Report ORNL-6895. Oak Ridge National Laboratory, Tennessee, USA.

Caglar, S., Saykal, T., Buyukgungor, O. & Sahin, E. (2014). *Synth. React. Inorg. Met.-Org. Nano-Met. Chem.* **44**, 1234–1242.

Çolak, A. T., Günay, H., Temel, E., Büyükgüngör, O. & Çolak, F. (2017). *Transit. Met. Chem.* **42**, 85–93.

Comba, P. & Remenyi, R. (2003). *Coord. Chem. Rev.* **238**, 9–20.

Farrugia, L. J. (2012). *J. Appl. Cryst.* **45**, 849–854.

Groom, C. R., Bruno, I. J., Lightfoot, M. P. & Ward, S. C. (2016). *Acta Cryst.* B**72**, 171–179.

Gross, E. U. K., Dobson, J. F. & Petersilka, M. (1996). *Density Functional Theory of Time Dependent Phenomena* in *Topics in Current Chemistry – Density Functional Theory II*, edited by K. Hafner, K. N. Houk, I. J. M. Lehn, K. N. Raymond, C. W. Rees, J. Thiem & F. Vogtle, pp. 81–172. Berlin: Springer.

Gross, E. K. U. & Kohn, W. (1990). *Adv. Quantum Chem.* **21**, 255–291.

Hamamci, S., Yilmaz, V. T. & Thöne, C. (2002). *Acta Cryst.* E**58**, m700–m701.

Huang, Q.-Y., Yang, Y. & Meng, X.-R. (2015). *Acta Cryst.* C**71**, 701–705.

Kelley, T. W., Baude, P. F., Gerlach, C., Ender, D. E., Muyres, D., Haase, M. A., Vogel, D. E. & Theiss, S. D. (2004). *Chem. Mater.* **16**, 4413–4422.

Kim, Y.-I., Song, Y.-K., Kim, D. & Kang, S. K. (2015). *Acta Cryst.* C**71**, 908–911.

Kong, L.-Q., Ju, X.-P. & Li, D.-C. (2009). *Acta Cryst.* E**65**, m1518.

Lapanje, K., Leban, I. & Lah, N. (2012). *Acta Cryst.* E**68**, m599.

Leitl, M. J., Zink, D. M., Schinabeck, A., Baumann, T., Volz, D. & Yersin, H. (2016). *Top Curr Chem (Z)*, **374**, 25–68.

Ley, A. N., Dunaway, L. E., Brewster, T. P., Dembo, M. D., Harris, T. D., Baril-Robert, F., Li, X., Patterson, H. H. & Pike, R. D. (2010). *Chem. Commun.* **46**, 4565–4567.
Lin, R.-G., Wang, Y.-L. & Liang, Q. (2015). *Acta Cryst.* C**71**, 44–47.
Macrae, C. F., Edgington, P. R., McCabe, P., Pidcock, E., Shields, G. P., Taylor, R., Towler, M. & van de Streek, J. (2006). *J. Appl. Cryst.* **39**, 453–457.
Martínez, A., Lorenzo, J., Prieto, M. J., Font-Bardia, M., Solans, X., Avilés, F. X. & Moreno, V. (2007). *Bioorg. Med. Chem.* **15**, 969–979.
Mobin, Sh. M., Srivastava, A. K., Mathur, P. & Lahiri, G. K. (2010). *Dalton Trans.* **39**, 1447–1449.
Perdew, J. P., Burke, K. & Ernzerhof, M. (1997). *Phys. Rev. Lett.* **78**, 1396–1396.
Pothiraja, R., Sathiyendiran, M., Steiner, A. & Murugavel, R. (2011). *Inorg. Chim. Acta*, **372**, 347–352.
Sheldrick, G. M. (2015). *Acta Cryst.* C**71**, 3–8.
Spek, A. L. (2009). *Acta Cryst*. D**65**, 148–155.
Stamatatos, T. C., Boudalis, A. K., Pringouri, K. V., Raptopoulou, C. P., Terzis, A., Wolowska, J., McInnes, E. J. L. & Perlepes, S. P. (2007). *Eur. J. Inorg. Chem.* pp. 5098–5104.
Trdin, M. & Lah, N. (2012). *Acta Cryst.* C**68**, m359–m362.
Trdin, M., Leban, I. & Lah, N. (2015). *Acta Chim. Slov.* **62**, 249–254.
Wang, F.-M., Lu, C.-S., Li, Y.-Z. & Meng, Q.-J. (2010). *Acta Cryst.* E**66**, m594.
Yeşılel, O. Z., Erer, H., Soylu, M. S. & Büyükgüngör, O. (2009). *J. Coord. Chem.* **62**, 2438–2448.
Yilmaz, V. T., Hamamci, S. & Thöne, C. (2003). *J. Coord. Chem.* **56**, 787–795.
Yilmaz, V. T., Yilmaz, F., Guney, E. & Buyukgungor, O. (2011). *J. Coord. Chem.* **64**, 159–169.
Zeghouan, O., Bendjeddou, L., Dems, M. A. & Merazig, H. (2016). Private communication (refcode 1481676). CCDC, Cambridge, England.
Zeghouan, O., Guenifa, F., Hadjadj, N., Bendjeddou, L. & Merazig, H. (2013). *Acta Cryst.* E**69**, m439–m440.
Zienkiewicz-Machnik, M., Masternak, J., Kazimierczuk, K. & Barszcz, B. (2016). *J. Mol. Struct.* **1126**, 37–46.

supporting information

Acta Cryst. (2018). E**74**, 1042-1048 [https://doi.org/10.1107/S2056989018009301]

A strongly fluorescent Ni^{II} complex with 2-(2-hydroxyethyl)pyridine ligands: synthesis, characterization and theoretical analysis and comparison with a related polymeric Cu^{II} complex

Ouahida Zeghouan, Mohamed AbdEsselem Dems, Seifeddine Sellami, Hocine Merazig and Jean Claude Daran

Computing details

Data collection: *APEX2* (Bruker, 2006); cell refinement: *SAINT* (Bruker, 2006); data reduction: *SAINT* (Bruker, 2006); program(s) used to solve structure: *SIR2002* (Burla *et al.*, 2003); program(s) used to refine structure: *SHELXL* (Sheldrick, 2015); molecular graphics: *ORTEPIII* (Burnett & Johnson, 1996), *ORTEP-3 for Windows* (Farrugia, 2012), *PLATON* (Spek, 2009); software used to prepare material for publication: *WinGX* (Farrugia, 2012) and *Mercury* (Macrae *et al.*, 2006).

Diaquabis[2-(2-hydroxyethyl)pyridine-κ^2N,O)nickel(II) dinitrate

Crystal data

$[Ni(C_7H_9NO)_2(H_2O)_2](NO_3)_2$
M_r = 465.05
Triclinic, $P\overline{1}$
Hall symbol: -P 1
a = 7.782 (5) Å
b = 8.185 (5) Å
c = 8.811 (5) Å
α = 96.785 (5)°
β = 113.856 (5)°
γ = 109.140 (5)°
V = 464.0 (5) Å^3
Z = 1
$F(000)$ = 242
D_x = 1.664 Mg m^{-3}
Mo $K\alpha$ radiation, λ = 0.71073 Å
Cell parameters from 1536 reflections
θ = 2.8–33.8°
μ = 1.11 mm^{-1}
T = 293 K
Prism, green
0.18 × 0.11 × 0.08 mm

Data collection

Bruker APEXII diffractometer
Radiation source: fine-focus sealed tube
Graphite monochromator
φ scans
2478 measured reflections
2478 independent reflections
2471 reflections with $I > 2\sigma(I)$
R_{int} = 0.019
θ_{max} = 29.1°, θ_{min} = 3.0°
h = −11→11
k = −11→11
l = −12→11

Refinement

Refinement on F^2
Least-squares matrix: full
$R[F^2 > 2\sigma(F^2)]$ = 0.018
$wR(F^2)$ = 0.051
S = 1.08
2478 reflections
133 parameters
4 restraints

Hydrogen site location: mixed
H atoms treated by a mixture of independent and constrained refinement

$w = 1/[\sigma^2(F_o^2) + (0.0235P)^2 + 0.1863P]$ where $P = (F_o^2 + 2F_c^2)/3$
$(\Delta/\sigma)_{max} < 0.001$
$\Delta\rho_{max} = 0.42$ e Å^{-3}
$\Delta\rho_{min} = -0.29$ e Å^{-3}

Special details

Geometry. All esds (except the esd in the dihedral angle between two l.s. planes) are estimated using the full covariance matrix. The cell esds are taken into account individually in the estimation of esds in distances, angles and torsion angles; correlations between esds in cell parameters are only used when they are defined by crystal symmetry. An approximate (isotropic) treatment of cell esds is used for estimating esds involving l.s. planes.

Fractional atomic coordinates and isotropic or equivalent isotropic displacement parameters (Å²)

	x	*y*	*z*	U_{iso}*/U_{eq}
Ni1	0.500000	0.500000	1.000000	0.01030 (6)
O1W	0.76119 (11)	0.49746 (9)	0.98827 (9)	0.01538 (14)
H2W	0.870471	0.591206	1.051410	0.023*
H1W	0.786623	0.405991	1.002286	0.023*
O1	0.36368 (11)	0.22139 (9)	0.92461 (9)	0.01563 (14)
H1	0.312496	0.167495	0.978813	0.023*
O3	0.88841 (12)	0.18215 (11)	0.80898 (10)	0.02212 (16)
O4	0.81394 (14)	0.18243 (11)	1.02219 (11)	0.02427 (17)
O2	0.77192 (14)	−0.06798 (10)	0.86796 (11)	0.02611 (18)
N1	0.36503 (12)	0.49127 (11)	0.73709 (10)	0.01265 (15)
N2	0.82483 (13)	0.09922 (11)	0.89982 (11)	0.01520 (16)
C2	0.26126 (17)	0.10590 (13)	0.75001 (13)	0.01930 (19)
H2B	0.116946	0.085298	0.694728	0.023*
H2A	0.268633	−0.009987	0.751370	0.023*
C3	0.36373 (16)	0.19383 (13)	0.64843 (13)	0.01691 (18)
H3A	0.511649	0.232402	0.715215	0.020*
H3B	0.315995	0.104372	0.541211	0.020*
C7	0.24432 (16)	0.64650 (14)	0.52920 (13)	0.01830 (19)
H7	0.220254	0.747349	0.506920	0.022*
C6	0.20270 (16)	0.50690 (15)	0.39547 (13)	0.01914 (19)
H6	0.151505	0.513073	0.281924	0.023*
C8	0.32254 (15)	0.63218 (13)	0.69660 (12)	0.01527 (17)
H8	0.346937	0.724379	0.785476	0.018*
C4	0.32151 (14)	0.35408 (13)	0.60574 (12)	0.01359 (17)
C5	0.23876 (16)	0.35837 (14)	0.43420 (12)	0.01737 (18)
H5	0.207865	0.261841	0.346023	0.021*

Atomic displacement parameters (Å²)

	U^{11}	U^{22}	U^{33}	U^{12}	U^{13}	U^{23}
Ni1	0.01338 (8)	0.00887 (8)	0.00873 (8)	0.00453 (6)	0.00534 (6)	0.00257 (6)
O1W	0.0160 (3)	0.0134 (3)	0.0175 (3)	0.0064 (3)	0.0085 (3)	0.0041 (3)
O1	0.0221 (3)	0.0099 (3)	0.0129 (3)	0.0034 (3)	0.0092 (3)	0.0027 (2)
O3	0.0254 (4)	0.0203 (4)	0.0214 (4)	0.0055 (3)	0.0140 (3)	0.0093 (3)

O4	0.0394 (5)	0.0201 (4)	0.0242 (4)	0.0169 (3)	0.0210 (4)	0.0073 (3)
O2	0.0401 (5)	0.0120 (3)	0.0290 (4)	0.0060 (3)	0.0232 (4)	0.0038 (3)
N1	0.0150 (3)	0.0124 (3)	0.0109 (3)	0.0058 (3)	0.0062 (3)	0.0035 (3)
N2	0.0148 (4)	0.0143 (4)	0.0157 (4)	0.0055 (3)	0.0069 (3)	0.0042 (3)
C2	0.0266 (5)	0.0106 (4)	0.0149 (4)	0.0034 (4)	0.0088 (4)	0.0006 (3)
C3	0.0241 (5)	0.0144 (4)	0.0140 (4)	0.0097 (4)	0.0097 (4)	0.0026 (3)
C7	0.0214 (5)	0.0195 (5)	0.0160 (4)	0.0103 (4)	0.0081 (4)	0.0090 (4)
C6	0.0200 (4)	0.0248 (5)	0.0116 (4)	0.0086 (4)	0.0065 (4)	0.0072 (4)
C8	0.0186 (4)	0.0144 (4)	0.0136 (4)	0.0076 (3)	0.0075 (3)	0.0046 (3)
C4	0.0144 (4)	0.0139 (4)	0.0121 (4)	0.0049 (3)	0.0069 (3)	0.0026 (3)
C5	0.0188 (4)	0.0198 (4)	0.0111 (4)	0.0065 (4)	0.0067 (3)	0.0018 (3)

Geometric parameters (Å, º)

Ni1—O1^{i}	2.0622 (14)	C2—C3	1.5193 (15)
Ni1—O1	2.0622 (14)	C2—H2B	0.9700
Ni1—O1W^{i}	2.0831 (15)	C2—H2A	0.9700
Ni1—O1W	2.0831 (15)	C3—C4	1.5063 (15)
Ni1—N1	2.1019 (14)	C3—H3A	0.9700
Ni1—N1^{i}	2.1019 (14)	C3—H3B	0.9700
O1W—H2W	0.8426	C7—C8	1.3861 (15)
O1W—H1W	0.8451	C7—C6	1.3891 (16)
O1—C2	1.4374 (14)	C7—H7	0.9300
O1—H1	0.8184	C6—C5	1.3848 (16)
O3—N2	1.2548 (12)	C6—H6	0.9300
O4—N2	1.2537 (12)	C8—H8	0.9300
O2—N2	1.2520 (14)	C4—C5	1.3930 (15)
N1—C8	1.3485 (14)	C5—H5	0.9300
N1—C4	1.3570 (13)		
O1^{i}—Ni1—O1	180.0	O1—C2—C3	109.66 (9)
O1^{i}—Ni1—O1W^{i}	90.74 (4)	O1—C2—H2B	109.7
O1—Ni1—O1W^{i}	89.26 (4)	C3—C2—H2B	109.7
O1^{i}—Ni1—O1W	89.26 (4)	O1—C2—H2A	109.7
O1—Ni1—O1W	90.74 (4)	C3—C2—H2A	109.7
O1W^{i}—Ni1—O1W	180.0	H2B—C2—H2A	108.2
O1^{i}—Ni1—N1	91.32 (3)	C4—C3—C2	113.88 (9)
O1—Ni1—N1	88.68 (3)	C4—C3—H3A	108.8
O1W^{i}—Ni1—N1	90.00 (4)	C2—C3—H3A	108.8
O1W—Ni1—N1	90.00 (4)	C4—C3—H3B	108.8
O1^{i}—Ni1—N1^{i}	88.68 (3)	C2—C3—H3B	108.8
O1—Ni1—N1^{i}	91.32 (3)	H3A—C3—H3B	107.7
O1W^{i}—Ni1—N1^{i}	90.00 (4)	C8—C7—C6	118.53 (10)
O1W—Ni1—N1^{i}	90.00 (4)	C8—C7—H7	120.7
N1—Ni1—N1^{i}	180.0	C6—C7—H7	120.7
Ni1—O1W—H2W	114.9	C5—C6—C7	118.83 (10)
Ni1—O1W—H1W	117.1	C5—C6—H6	120.6
H2W—O1W—H1W	108.6	C7—C6—H6	120.6

C2—O1—Ni1	125.84 (6)	N1—C8—C7	123.30 (9)
C2—O1—H1	107.8	N1—C8—H8	118.3
Ni1—O1—H1	120.3	C7—C8—H8	118.3
C8—N1—C4	117.93 (9)	N1—C4—C5	121.60 (9)
C8—N1—Ni1	118.03 (6)	N1—C4—C3	118.57 (9)
C4—N1—Ni1	124.03 (7)	C5—C4—C3	119.83 (9)
O2—N2—O4	119.76 (9)	C6—C5—C4	119.75 (9)
O2—N2—O3	119.70 (9)	C6—C5—H5	120.1
O4—N2—O3	120.54 (9)	C4—C5—H5	120.1

Symmetry code: (i) −*x*+1, −*y*+1, −*z*+2.

Hydrogen-bond geometry (Å, º)

D—H···*A*	*D*—H	H···*A*	*D*···*A*	*D*—H···*A*
O1*W*—H2*W*···O3^{ii}	0.84	1.95	2.7870 (16)	176
O1*W*—H2*W*···N2^{ii}	0.84	2.68	3.455 (2)	153
O1*W*—H1*W*···O4	0.85	1.93	2.7720 (19)	174
O1—H1···O2^{iii}	0.82	1.88	2.6952 (15)	172
O1—H1···N2^{iii}	0.82	2.65	3.4208 (17)	159
C2—H2*B*···O3^{iv}	0.97	2.64	3.378 (2)	133
C3—H3*A*···O1*W*	0.97	2.55	3.2278 (17)	127
C8—H8···O1^{i}	0.93	2.49	3.0136 (19)	116
C8—H8···O4^{i}	0.93	2.66	3.4448 (18)	143
C5—H5···O2^{v}	0.93	2.41	3.3076 (19)	163

Symmetry codes: (i) −*x*+1, −*y*+1, −*z*+2; (ii) −*x*+2, −*y*+1, −*z*+2; (iii) −*x*+1, −*y*, −*z*+2; (iv) *x*−1, *y*, *z*; (v) −*x*+1, −*y*, −*z*+1.